The Astrophysical Journal, 959:141 (11pp), 2023 December 20 https://doi.org/10.3847/1538-4357/ad0385
© 2023. The Author(s). Published by the American Astronomical Society.
OPEN ACCESS

Chemical Analysis of the Brightest Star of the Cetus II Ultrafaint Dwarf Galaxy Candidate*

K. B. Webber[1], T. T. Hansen[2], J. L. Marshall[1], J. D. Simon[3], A. B. Pace[4], B. Mutlu-Pakdil[5], A. Drlica-Wagner[6,7,8], C. E. Martínez-Vázquez[9,10], M. Aguena[11], S. S. Allam[6], O. Alves[12], E. Bertin[13,14], D. Brooks[15], A. Carnero Rosell[11,16,17], J. Carretero[18], L. N. da Costa[11], J. De Vicente[19], P. Doel[15], I. Ferrero[20], D. Friedel[21], J. Frieman[6,7], J. García-Bellido[22], G. Giannini[18], D. Gruen[23], R. A. Gruendl[21,24], S. R. Hinton[25], D. L. Hollowood[26], K. Honscheid[27,28], K. Kuehn[29,30], J. Mena-Fernández[19], F. Menanteau[21,24], R. Miquel[18,31], R. L. C. Ogando[32], M. E. S. Pereira[33], A. Pieres[11,32], A. A. Plazas Malagón[34,35], E. Sanchez[19], B. Santiago[11,36], J. Allyn Smith[37], M. Smith[38], E. Suchyta[39], G. Tarle[12], C. To[27], N. Weaverdyck[12,40], and B. Yanny[6]

[1] Mitchell Institute for Fundamental Physics and Astronomy and Department of Physics and Astronomy, Texas A&M University, College Station, TX 77843-4242, USA; kbwebber@tamu.edu
[2] Department of Astronomy, Stockholm University, AlbaNova University Center, SE-106 91 Stockholm, Sweden
[3] Observatories of the Carnegie Institution for Science, 813 Santa Barbara St., Pasadena, CA 91101, USA
[4] McWilliams Center for Cosmology, Carnegie Mellon University, 5000 Forbes Ave., Pittsburgh, PA 15213, USA
[5] Department of Physics and Astronomy, Dartmouth College, Hanover, NH 03755, USA
[6] Fermi National Accelerator Laboratory, P.O. Box 500, Batavia, IL 60510, USA
[7] Kavli Institute for Cosmological Physics, University of Chicago, Chicago, IL 60637, USA
[8] Department of Astronomy and Astrophysics, University of Chicago, Chicago, IL 60637, USA
[9] Gemini Observatory, NSF's NOIRLab, 670 N. A'ohoku Pl., Hilo, HI 96720, USA
[10] Cerro Tololo Inter-American Observatory, NSF's NOIRLab, Casilla 603, La Serena, Chile
[11] Laboratório Interinstitucional de e-Astronomia—LIneA, Rua Gal. José Cristino 77, Rio de Janeiro, RJ—20921-400, Brazil
[12] Department of Physics, University of Michigan, Ann Arbor, MI:48109, USA
[13] CNRS, UMR 7095, Institut d'Astrophysique de Paris, F-75014, Paris, France
[14] Sorbonne Universités, UPMC Univ Paris 06, UMR 7095, Institut d'Astrophysique de Paris, F-75014, Paris, France
[15] Department of Physics & Astronomy, University College London, Gower St., London, WC1E 6BT, UK
[16] Instituto de Astrofisica de Canarias, E-38205 La Laguna, Tenerife, Spain
[17] Universidad de La Laguna, Dpto. Astrofísica, E-38206 La Laguna, Tenerife, Spain
[18] Institut de Física d'Altes Energies (IFAE), The Barcelona Institute of Science and Technology, Campus UAB, E-08193 Bellaterra Barcelona, Spain
[19] Centro de Investigaciones Energéticas, Medioambientales y Tecnológicas (CIEMAT), Madrid, Spain
[20] Institute of Theoretical Astrophysics, University of Oslo.P.O. Box 1029 Blindern, NO-0315 Oslo, Norway
[21] Center for Astrophysical Surveys, National Center for Supercomputing Applications, 1205 West Clark St., Urbana, IL 61801, USA
[22] Instituto de Fisica Teorica UAM/CSIC, Universidad Autonoma de Madrid, E-28049 Madrid, Spain
[23] University Observatory, Faculty of Physics, Ludwig-Maximilians-Universität, Scheinerstr. 1, D-81679 Munich, Germany
[24] Department of Astronomy, University of Illinois at Urbana-Champaign, 1002 W. Green St., Urbana, IL 61801, USA
[25] School of Mathematics and Physics, University of Queensland, Brisbane, QLD 4072, Australia
[26] Santa Cruz Institute for Particle Physics, Santa Cruz, CA 95064, USA
[27] Center for Cosmology and Astro-Particle Physics, The Ohio State University, Columbus, OH 43210, USA
[28] Department of Physics, The Ohio State University, Columbus, OH 43210, USA
[29] Australian Astronomical Optics, Macquarie University, North Ryde, NSW 2113, Australia
[30] Lowell Observatory, 1400 Mars Hill Rd., Flagstaff, AZ 86001, USA
[31] Institució Catalana de Recerca i Estudis Avançats, E-08010 Barcelona, Spain
[32] Observatório Nacional, Rua Gal. José Cristino 77, Rio de Janeiro, RJ—20921-400, Brazil
[33] Hamburger Sternwarte, Universität Hamburg, Gojenbergsweg 112, D-21029 Hamburg, Germany
[34] Kavli Institute for Particle Astrophysics & Cosmology, P.O. Box 2450, Stanford University, Stanford, CA 94305, USA
[35] SLAC National Accelerator Laboratory, Menlo Park, CA 94025, USA
[36] Instituto de Física, UFRGS, Caixa Postal 15051, Porto Alegre, RS—91501-970, Brazil
[37] Austin Peay State University, Dept. Physics, Engineering and Astronomy, P.O. Box 4608 Clarksville, TN 37044, USA
[38] School of Physics and Astronomy, University of Southampton, Southampton, SO17 1BJ, UK
[39] Computer Science and Mathematics Division, Oak Ridge National Laboratory, Oak Ridge, TN 37831, USA
[40] Lawrence Berkeley National Laboratory, 1 Cyclotron Rd., Berkeley, CA 94720, USA
Received 2023 July 18; revised 2023 October 4; accepted 2023 October 9; published 2023 December 15

Abstract

We present a detailed chemical abundance analysis of the brightest star in the ultrafaint dwarf (UFD) galaxy candidate Cetus II from high-resolution Magellan/MIKE spectra. For this star, DES J011740.53-173053, abundances or upper limits of 18 elements from carbon to europium are derived. Its chemical abundances generally follow those of other UFD galaxy stars, with a slight enhancement of the α-elements (Mg, Si, and Ca) and low neutron-capture element (Sr, Ba, and Eu) abundances supporting the classification of Cetus II as a likely UFD. The

* This paper includes data gathered with the 6.5 m Magellan Telescopes located at Las Campanas Observatory, Chile.

Original content from this work may be used under the terms of the Creative Commons Attribution 4.0 licence. Any further distribution of this work must maintain attribution to the author(s) and the title of the work, journal citation and DOI.

star exhibits lower Sc, Ti, and V abundances than Milky Way (MW) halo stars with similar metallicity. This signature is consistent with yields from a supernova originating from a star with a mass of $\sim$11.2 $M_{\odot}$. In addition, the star has a potassium abundance of [K/Fe] = 0.81, which is somewhat higher than the K abundances of MW halo stars with similar metallicity, a signature that is also present in a number of UFD galaxies. A comparison including globular clusters and stellar stream stars suggests that high K is a specific characteristic of some UFD galaxy stars and can thus be used to help classify objects as UFD galaxies.

Unified Astronomy Thesaurus concepts: Chemical abundances (224); Stellar abundances (1577)

Supporting material: machine-readable table

1. Introduction

Stars maintain in their atmospheres a fingerprint of the chemical composition of their birth environment and thereby also contain information about the stellar generations that were present before them. They can therefore be used to study the chemical enrichment, which is a useful probe for characterizing the nature of the stellar environment. Variations in chemical abundances across different stellar associations can give insight into properties such as different timescales for chemical enrichment and variations in stellar initial mass functions.

In recent years, photometric surveys such as the Dark Energy Survey and Pan-STARRS (The Dark Energy Survey Collaboration 2005; Bechtol et al. 2015; Drlica-Wagner et al. 2015; Koposov et al. 2015; Laevens et al. 2015) have detected a large number of stellar overdensities around the Milky Way (MW). In the process of characterizing these systems, chemical abundance analysis has proven to be a valuable tool for discerning the physical nature of the associations and sometimes reveals unusual chemical abundance patterns. Although further observations of a few of these overdensities have determined that they are not genuine physical objects (Cantu et al. 2021), nearly all of the overdensities have been found to be either star clusters or ultrafaint dwarf (UFD) galaxies (Laevens et al. 2014; Luque et al. 2018; Simon 2019).

Star clusters can be sorted into different categories: stellar associations, open clusters, or globular clusters (GCs; Trumpler 1930; Krumholz et al. 2019). Each of these types of systems has distinguishing features in the abundances of their member stars that can be used to identify the type of cluster. Open clusters are homogeneous in the abundances of all elements, while GCs are not fully homogeneous (Krumholz et al. 2019). GCs are also known to display specific anticorrelations between certain elements such as Mg–Al and Na–O (Carretta et al. 2010; Mucciarelli et al. 2018). Hence, the study of the chemical enrichment of star clusters can yield useful information about the nature of these objects and aid in their classification.

Ultrafaint dwarf galaxies are low-mass, low-luminosity galaxies that are dominated by dark matter (Simon & Geha 2007). The current stellar population of UFD galaxies is very old ($\sim$10 Gyr) and metal-poor ([Fe/H] < -1.4, Simon 2019), with abundances reflecting the elements created by the first generation of stars. Studying the abundances of stars in UFD galaxies therefore provides a window for studying the nucleosynthetic processes of the early Universe. Furthermore, the UFD galaxies are small, isolated systems and reflect the chemical signatures of a few nucleosynthetic events (Ji et al. 2016; Hansen et al. 2017, 2020; Marshall et al. 2019).

Previous studies of stellar abundances in UFD galaxies have found generally similar abundance patterns from one system to the next (Frebel & Norris 2015), with most of the stars exhibiting a slight enhancement of the α-elements (Mg, Si, and Ca; Frebel et al. 2010; Lai et al. 2011; Simon 2019), as seen for metal-poor stars in the MW halo (e.g., McWilliam 1998; Cayrel et al. 2004), reflecting enrichment by core-collapse supernova (SN). In addition, and specific to UFD galaxies, most systems also display very low neutron-capture element abundances (e.g., Ji et al. 2019). With the increase in the number of systems that are discovered and analyzed, more variation in the abundances has begun to appear. Examples of systems with unusual abundance patterns include Reticulum II, where $\sim$72% of the analyzed stars show an enhancement in neutron-capture elements, likely due to a neutron star merger event that occurred early in the history of the galaxy (Ji et al. 2016, 2022; Roederer et al. 2016), and Grus II, where all three analyzed stars have a higher [Mg/Ca] ratio than other UFD galaxies, which indicates that a top-heavy initial mass function governs the early star formation in this galaxy (Hansen et al. 2020).

In this paper, we present a detailed chemical abundance analysis of the brightest star of the Cetus II (Cet II) UFD galaxy candidate, DES J011740.53–173053.1 (hereafter J0117). Cet II was discovered as a stellar overdensity in the Dark Energy Survey at a heliocentric distance of 30 kpc (Drlica-Wagner et al. 2015). At the time of discovery, Cet II was the faintest and smallest candidate UFD galaxy system detected, making it difficult to determine the velocity and metallicity dispersion. The brightest member therefore was a prime target for high-resolution follow-up for an abundance analysis. As described above, both UFD galaxies and star clusters have distinct chemical features that can be used to classify the system. Hence a detailed chemical analysis is the natural next step in the efforts to characterize the Cet II system.

The outline of the paper is as follows. In Section 2, the observations are described, and in Section 3, the stellar parameters and analysis are detailed. Section 4 presents our results that are further discussed in Section 5. Section 6 provides a summary.

2. Observations

Based on medium-resolution spectroscopy of the Cet II field obtained with the Magellan/IMACS spectrograph (Dressler et al. 2011) in 2016, we identified a set of likely Cet II member stars centered at a velocity of $V_{\rm helio} = -82$ km s^{-1}. Subsequently, Pace & Li (2019) and Pace et al. (2022) showed that these stars also share a common proper motion, confirming that they are associated with Cet II. Surprisingly, given the low stellar mass of Cet II, one of the member stars is located on the upper red giant branch at an apparent magnitude of $g = 16.44$, $\sim$3 mag brighter than any other Cet II stars. This bright star, J0117, was then an obvious target for high-resolution spectroscopy to investigate the chemical abundances in Cet II.

High-resolution spectral data were obtained for J0117 with the MIKE echelle spectrograph at Las Campanas Observatory

Table 1
Observing Details and Stellar Data

ID	R.A.	Decl.	g_0 (mag)	r_0 (mag)	i_0 (mag)	z_0 (mag)	HJD	Exp Time (s)	S/N @ 4500 Å	$V_{\rm helio} \pm \sigma$ (km s^{-1})
J0117	01:17:40.9	−17:30:54.5	16.443	15.716	15.818	16.014	2457988.70127	2 × 1800	15	−81.38 ± 0.52
							2458059.49903	5 × 1800	21	−81.89 ± 0.51

Note. HJD values at the beginning of the exposure.

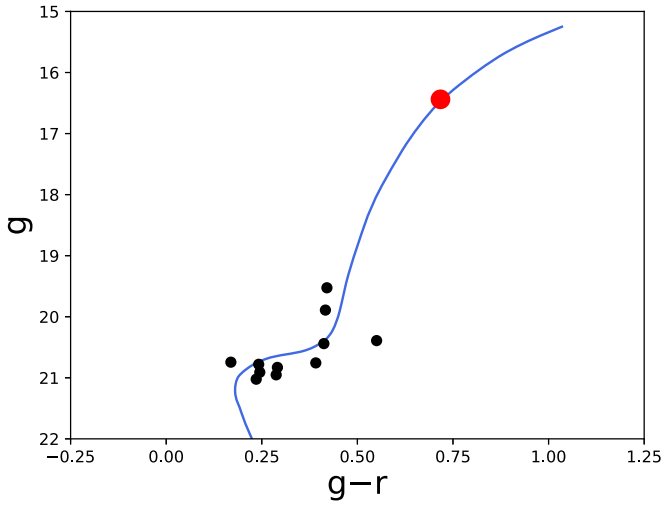

Figure 1. Color–magnitude diagram for Cetus II. The black dots are stars with a membership probability $p > 0.01$ (Pace et al. 2022), and the red dot is J0117. The blue line shows a Dartmouth isochrone (Dotter et al. 2008) with [Fe/H] = − 2.3 and age = 12.5 Gyr, transformed to the DES photometric system (Drlica-Wagner et al. 2018) and shifted to the distance of Cetus II (∼30 kpc; Drlica-Wagner et al. 2015).

in Chile (Bernstein et al. 2003) in 2017 August and November. A color–magnitude diagram of Cet II member stars (Pace et al. 2022) is shown in Figure 1. J0117 is marked with a red dot and is notably brighter than the other currently known members.

Right ascension, declination, and dereddened DES magnitudes for J0117 are listed in Table 1, along with Heliocentric Julian Date (HJD), exposure times, the signal-to-noise ratio per pixel (S/N), and the heliocentric radial velocities for the spectra. The spectra were obtained using a 0.″7 slit with 2 × 2 pixel binning and cover a wavelength range of 3350–5000 Å in the blue and 4900–9500 Å in the red, with resolutions ($R = \lambda/\Delta\lambda$) of $R \sim 35{,}000$ at blue wavelengths and ∼28,000 at red wavelengths, respectively. The data from each observing run were reduced using the CarPy MIKE pipeline (Kelson et al. 2000; Kelson 2003), and the spectra from the two runs were subsequently coadded. The heliocentric radial velocity of the star was determined by cross-correlation with a spectrum of the bright metal-poor red giant HD122563 ($V_{\rm helio} = -26.17$ km s^{-1}; Gaia Collaboration et al. 2021). Thirty-six echelle orders were used for the correlation in each spectrum, yielding mean radial velocities of −81.38 and −81.89 km s^{-1} for the two spectra. Since there is no appreciable variation in the radial velocities between the two spectra, this star is likely not a short-period binary.

3. Stellar Parameters and Abundance Analysis

Stellar parameters and abundances were derived from equivalent width (EW) measurements and spectral synthesis using the program Spectroscopy Made Hard(er) (SMHR[41]), which runs the 2017 version of the radiative transfer code MOOG[42] (Sneden 1973; Sobeck et al. 2011) assuming local thermodynamical equilibrium (LTE). One-dimensional (1D) α-enhanced ([α/Fe] = +0.4) ATLAS model atmospheres (Castelli & Kurucz 2003) were used as input, with line lists generated from linemake, which include hyperfine structure and isotopic shifts where applicable[43] (Placco et al. 2021), and solar abundances were taken from Asplund et al. (2009). For the derivation of Ba, we used the *r*-process isotopic ratio from Sneden et al. (2008).

The stellar parameters effective temperature ($T_{\rm eff}$), surface gravity ($\log g$), metallicity ([Fe/H]), and microturbulence (ξ) were determined spectroscopically using EW measurements of 95 Fe I and 7 Fe II lines (see Table 2). The EWs of the Fe I and Fe II lines were measured by fitting Gaussian profiles to the absorption features in the continuum-normalized spectra. Using these measurements, $T_{\rm eff}$ was derived from the excitation equilibrium of the Fe I lines and then corrected for the offset between spectroscopic and photometric temperature scales using the method outlined in Frebel et al. (2013). Next, $\log g$ was determined from the ionization balance between the Fe I

Table 2
Data for Atomic Lines Used in the Analysis and Individual Line EW Measurements

Species	λ (Å)	χ (eV)	$\log gf$	EW (mÅ)	$\sigma_{\rm EW}$ (mÅ)	$\log \epsilon$	ref
Na I	5889.95	0.00	0.11	197.33	2.83	4.04	1
Na I	5895.92	0.00	−0.19	171.34	2.89	3.99	1
Mg I	4167.27	4.35	−0.74	84.82	6.00	5.80	1
Mg I	4702.99	4.33	−0.44	95.81	2.96	5.54	1
Mg I	5172.68	2.71	−0.36	248.53	6.18	5.47	2

Note. The complete version of this table is available online only. A short version is shown here to illustrate its form and content.

References. (1) Kramida et al. (2018); (2) Pehlivan Rhodin et al. (2017); (3) Yu & Derevianko (2018); (4) Lawler & Dakin (1989), using hfs from Kurucz & Bell (1995); (5) Lawler et al. (2013); (6) = Wood et al. (2013); (7) Pickering et al. (2001), with corrections given in Pickering et al. (2002); (8) Lawler et al. (2014) for $\log gf$ values and HFS; (9) Wood et al. (2014) for $\log gf$ values and HFS, when available; (10) Sobeck et al. (2007); (11) Lawler et al. (2017); (12) Den Hartog et al. (2011) for both $\log gf$ value and hfs; (13) O'Brian et al. (1991); (14) Den Hartog et al. (2014); (15) Belmonte et al. (2017); (16) Ruffoni et al. (2014); (17) Den Hartog et al. (2019); (18) Meléndez & Barbuy (2009); (19) Lawler et al. (2015) for $\log gf$ values and HFS; (20) Wood et al. (2014); (21) Roederer & Lawler (2012); (22) Kramida et al. (2018), using HFS/IS from McWilliam (1998) when available.

(This table is available in its entirety in machine-readable form.)

[41] https://github.com/andycasey/smhr
[42] https://github.com/alexji/moog17scat
[43] https://github.com/vmplacco/linemake

Table 3
Stellar Model Atmosphere Parameters of J0117

	$T_{\rm eff}$ (K)	$\log g$ (cgs)	ξ (km s^{-1})	[Fe/H]
Value	4727	1.40	1.89	−2.09
Statistical uncertainties	41	0.07	0.07	0.17
Systematic uncertainties	150	0.3	0.2	0.12

and Fe II lines, and ξ was determined by removing any trend in line abundances with reduced equivalent width for the Fe I lines. The final stellar parameters are listed in Table 3. For comparison, a photometric temperature of 4592 ± 69 K for the star was also derived by converting the dereddened DES g, r, i, and z colors to B, V, R, and I colors (Drlica-Wagner et al. 2018, R. Lupton 2005[44]) and using the color-temperature relations from Casagrande et al. (2010). The photometric temperature is in good agreement with the corrected spectroscopic temperature. Following Frebel et al. (2013), we adopt a 150 K systematic uncertainty for $T_{\rm eff}$, corresponding to an uncertainty of 0.3 dex in $\log g$, 0.2 km s^{-1} in ξ, and 0.18 dex in [Fe/H]. The statistical uncertainties on $T_{\rm eff}$, $\log g$ and ξ were derived by varying each parameter to match the standard deviation of the Fe I lines as listed in Table 3. After the stellar parameters were determined, the elemental abundances were derived from EW measurements or spectral synthesis. EWs were used for lines that are not blended, while spectral synthesis was used for blended lines and/or lines that are affected by isotopic and/or hyperfine splitting. The atomic data, wavelength, excitation potential, and oscillator strength for individual lines used for the abundance determination are listed in Table 2. The table also lists the measured EWs, uncertainties on these, and the corresponding abundances for the lines used. The final weighted mean abundances and associated uncertainties were determined following the method outlined in Ji et al. (2020). This method uses a mean that is weighted by the S/N of the individual lines to calculate the final abundances and fully propagates statistical and systematic stellar parameter uncertainties for individual line measurements, including stellar parameter covariances, to determine the uncertainty.

4. Results

Abundances or upper limits have been derived for 18 elements from C to Eu in J0117. The LTE abundances and upper limits, along with the systematic abundance uncertainty (s_X) and uncertainties arising from stellar parameter uncertainties ($\Delta_{T_{\rm eff}}$, $\Delta_{\log g}$, Δ_{ξ}, and $\Delta_{\rm [Fe/H]}$), are presented in Table 4, where N is the number of lines for the given species. In Figures 2 and 3, we present a subset of elemental abundances for J0117 compared to abundances for stars in UFD galaxies (colored points) and metal-poor halo stars (gray points; Roederer et al. 2014). Data from the UFD galaxies are taken from Boötes I (Feltzing et al. 2009; Norris et al. 2010; Gilmore et al. 2013; Ishigaki et al. 2014; Frebel et al. 2016; Waller et al. 2022), Boötes II (Ji et al. 2016), Carina II (Ji et al. 2020), Carina III (Ji et al. 2020), Coma Berenices (Frebel et al. 2010; Waller et al. 2022), Grus I (Ji et al. 2019), Grus II (Hansen et al. 2020), Hercules (Koch et al. 2008), Horologium I (J. L. Marshall et al. 2023, in preparation), Leo IV (Simon et al. 2010), Pisces II (Spite et al. 2018), Reticulum II (Ji et al. 2016, 2019; Hayes et al. 2023), Segue 1 (Norris et al. 2010; Frebel et al. 2014), Segue 2 (Roederer & Kirby 2014), Triangulum II(Ji et al. 2019), Tucana II (Ji et al. 2016; Chiti et al. 2018, 2023), Tucana III (Hansen et al. 2017; Marshall et al. 2019), and Ursa Major II (Frebel et al. 2010).

4.1. Alpha Elements

We derive abundances for the α-elements Mg, Si, and Ca from EWs. We find a Mg I abundance of $[{\rm Mg\,I/Fe}] = 0.36 \pm 0.18$ from four Mg I absorption features, a Si I abundance of $[{\rm Si\,I/Fe}] = 0.59 \pm 0.24$ using three Si I lines, and a Ca I abundance of $[{\rm Ca\,I/Fe}] = 0.23 \pm 0.11$ from 20 Ca I lines. J0117 shows a general enhancement in α-elements as a result of enrichment by core-collapse SN, following the trend seen in metal-poor MW halo and other UFD galaxy stars (Frebel et al. 2010; Lai et al. 2011; Simon 2019).

4.2. Carbon and Odd-Z Elements

Abundances for C, Na, Al, K, and Sc were derived from EW and spectral synthesis analysis. A [C/Fe] of -0.31 ± 0.18 was determined from the CH G-band in regions around 4310 and 4230 Å via spectral synthesis. The C and O abundances are coupled through the CO molecule, and therefore, the O abundance of the star needs to be known to derive the C abundance. As we could not derive an O abundance for the star, we assumed a standard α-enhanced O abundance of $[{\rm O/Fe}] = 0.4$ for the spectral synthesis of CH because UFDs are known to be α-enhanced and J0117 is α-enhanced. The C abundance of a star is also altered as the star evolves. We used the tool from Placco et al. (2014) to determine a carbon correction of $\Delta[{\rm C/Fe}] = 0.57$ dex, resulting in an original C abundance of the star of $[{\rm C/Fe}] = 0.26$. A Na I abundance of $[{\rm Na\,I/Fe}] = 0.17 \pm 0.25$ and an Al I abundance of $[{\rm Al\,I/Fe}] = -0.33 \pm 0.41$ were derived from the EW analysis of the Na D resonance lines and two Al lines, respectively. The EW analysis of the two K lines at 7664 and 7698 Å was used to derive a K I abundance of $[{\rm K\,I/Fe}] = 0.81 \pm 0.25$. From the spectral synthesis of six Sc II lines, we derive a Sc II abundance of $[{\rm Sc\,II/Fe}] = -0.31 \pm 0.19$.

As can be seen in Figure 2, the C and Na abundances for J0117 follow those of other UFD galaxies and metal-poor MW halo stars. The Al abundance for J0117 may be slightly higher than what is seen in other UFD galaxies and metal-poor MW halo stars, but the uncertainty of ±0.41 is high. J0117 has an elevated K abundance compared to the average K abundances found in MW halo stars. In addition, J0117 exhibits a lower Sc abundance than what is found in most UFD galaxies and metal-poor MW halo stars.

4.3. Iron Peak Elements

The EW analysis was used to derive abundances for the iron peak elements Ti, Cr, Ni, and Zn and the spectral synthesis for the elements V, Mn, and Co. We identify 14 Ti I and 23 Ti II lines in the spectrum and find abundances of $[{\rm Ti\,I/Fe}] = -0.23 \pm 0.22$ and $[{\rm Ti\,II/Fe}] = 0.06 \pm 0.18$. V I and V II abundances were determined to be $[{\rm V\,I/Fe}] = -0.01 \pm 0.18$ and $[{\rm V\,II/Fe}] = 0.37 \pm 0.18$ from two and three lines, respectively, and Cr I and Cr II to be $[{\rm Cr\,I/Fe}] = -0.30 \pm 0.14$ and $[{\rm Cr\,II/Fe}] = -0.07 \pm 0.13$ from nine and two lines, respectively. There is a slight discrepancy between the abundances we derive

[44] http://www.sdss3.org/dr8/algorithms/sdssUBVRITransform.php

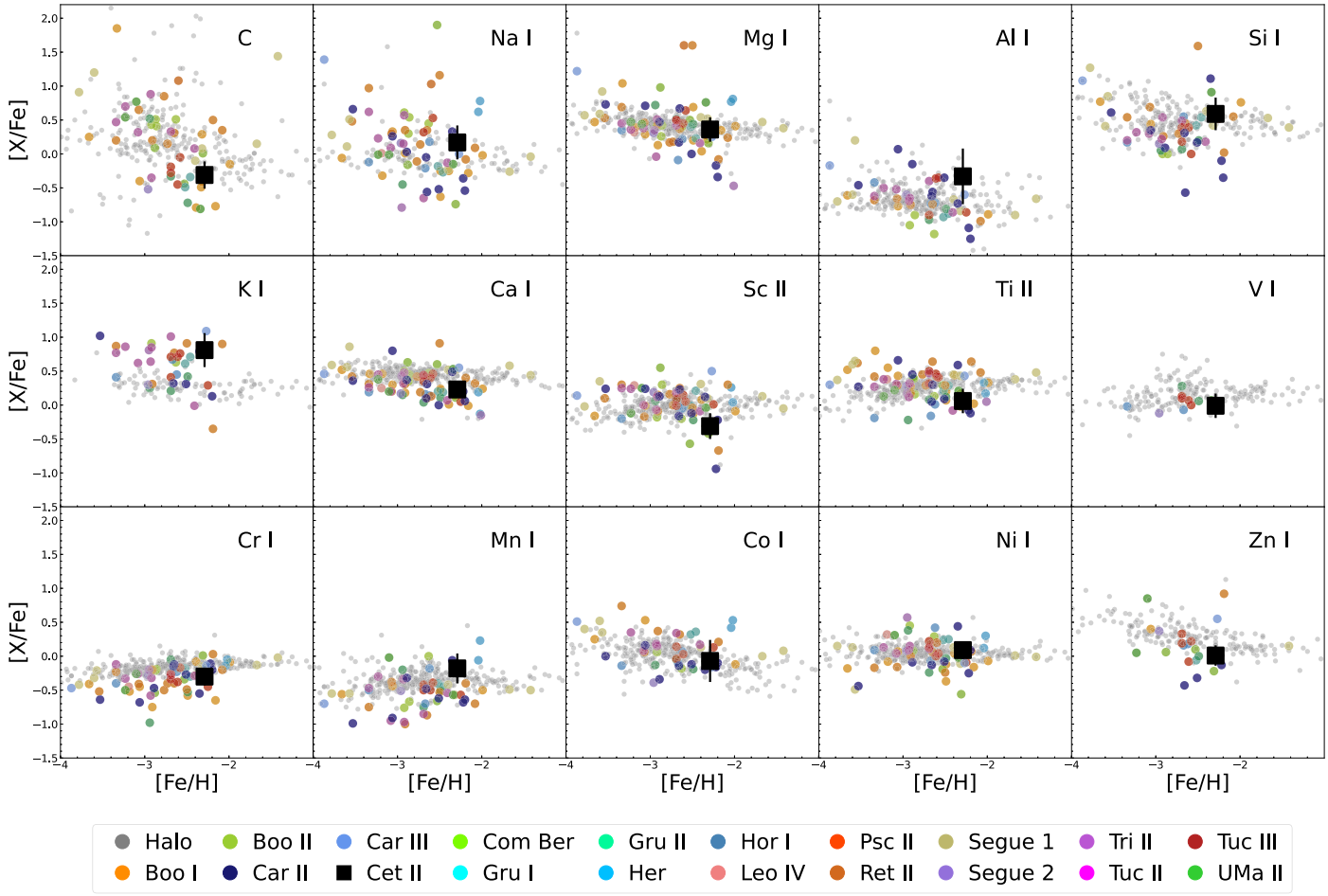

Figure 2. [X/Fe] derived abundances for J0117 (black square) compared to the abundances of UFD galaxies (colored dots; see text for references 4) and stars from the MW halo (gray dots; Roederer et al. 2014). J0117 follows the general abundance trends of what is seen in most UFD galaxy stars.

Table 4
Weighted Average Abundance Summary for J0117

El.	N	$\log \epsilon$	[X/H]	$\sigma_{[X/H]}$	[X/Fe]	$\sigma_{[X/Fe]}$	$\Delta_{T_{\rm eff}}$	$\Delta_{\log g}$	Δ_{ξ}	$\Delta_{[Fe/H]}$	s_X
CH	4	+5.85	−2.61	0.18	−0.31	0.18	0.29	−0.08	0.01	0.10	0.10
Na I	2	+4.02	−2.12	0.26	+0.17	0.25	0.26	−0.08	−0.14	−0.03	0.00
Mg I	4	+5.69	−1.93	0.17	+0.36	0.18	0.15	−0.07	−0.07	0.00	0.18
Al I	2	+3.79	−2.63	0.42	−0.33	0.41	0.25	−0.11	−0.11	−0.01	0.46
Si I	3	+5.86	−1.71	0.24	+0.59	0.24	0.18	−0.03	−0.06	−0.00	0.28
K I	2	+3.50	−1.49	0.26	+0.81	0.25	0.19	−0.03	−0.09	−0.02	0.09
Ca I	20	+4.38	−2.03	0.10	+0.23	0.11	0.15	−0.03	−0.06	−0.01	0.11
Sc II	6	+0.61	−2.61	0.19	−0.31	0.19	0.04	0.09	−0.07	0.03	0.10
Ti I	14	+2.64	−2.52	0.23	−0.23	0.22	0.25	−0.03	−0.05	−0.02	0.23
Ti II	23	+2.93	−2.23	0.17	+0.06	0.18	0.06	0.10	−0.11	0.04	0.28
V I	2	+1.64	−2.30	0.19	−0.01	0.18	0.17	−0.02	−0.01	−0.04	0.00
V II	3	+1.98	−1.93	0.17	+0.37	0.18	−0.02	0.12	−0.02	0.03	0.00
Cr I	9	+3.13	−2.59	0.14	−0.30	0.14	0.24	−0.03	−0.08	−0.02	0.08
Cr II	2	+3.29	−2.36	0.12	−0.07	0.13	−0.03	0.11	−0.02	0.02	0.00
Mn I	5	+2.97	−2.48	0.23	−0.18	0.22	0.20	−0.02	−0.08	−0.04	0.10
Fe I	95	+5.21	−2.29	0.08	⋯	⋯	0.07	−0.01	0.04	0.01	0.24
Fe II	7	+5.39	−2.22	0.15	⋯	⋯	−0.01	0.12	0.01	0.03	0.10
Co I	4	+2.73	−2.37	0.32	−0.07	0.31	0.25	0.00	−0.11	−0.04	0.00
Ni I	12	+4.12	−2.19	0.13	+0.09	0.13	0.17	−0.01	−0.04	−0.01	0.17
Zn I	1	+2.27	−2.29	0.15	+0.01	0.15	0.06	0.07	−0.02	0.02	0.00
Sr II	1	−1.52	−4.39	0.43	−2.10	0.43	0.07	0.12	−0.18	0.01	0.00
Ba II	1	−2.34	−4.52	0.39	−2.23	0.39	0.09	0.10	0.01	0.09	0.10
Eu II	1	< -1.92	< -2.44	⋯	< -0.33	⋯	⋯	⋯	⋯	⋯	⋯

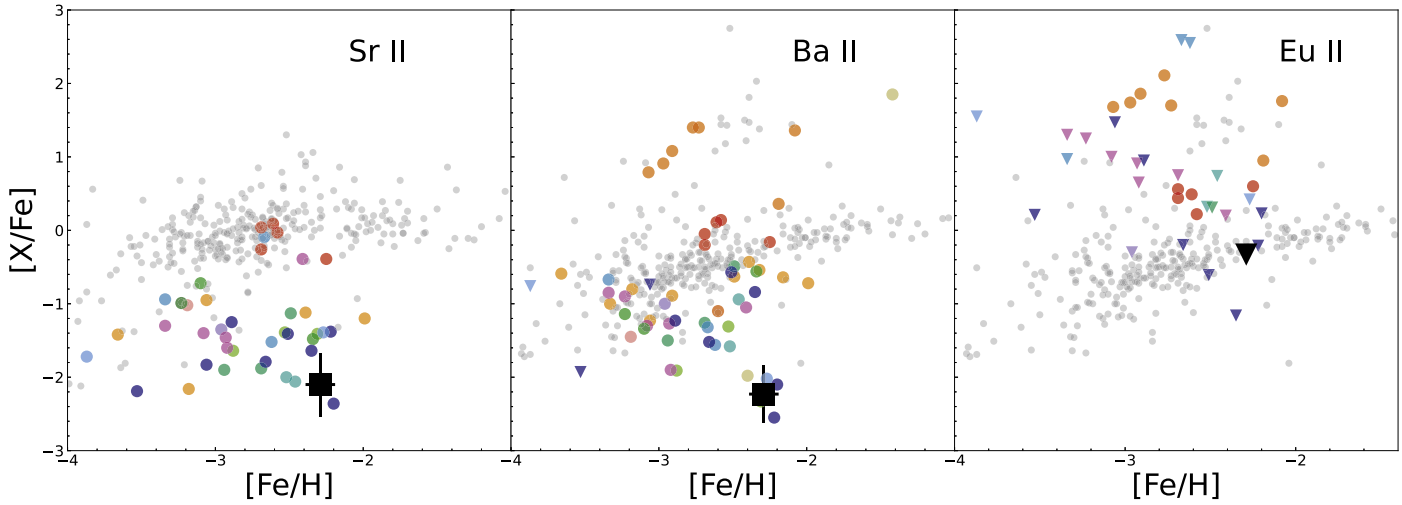

Figure 3. [X/Fe] derived neutron-capture element abundances for J0117 (black square) compared to the abundances of other UFD galaxies (colored dots; see text for references and Figure 2 for the legend) and stars from the MW halo (gray dots; Roederer et al. 2014). The upper limits are designated with downward-pointing triangles. J0117 has low abundances of neutron-capture elements, which is characteristic of most UFD galaxies.

from the neutral and ionized lines of the elements mentioned above, which may be due to the 1D LTE nature of the analysis. However, for most of the elements, the neutral and ionized abundances agree within the uncertainties. Finally, we derive Ni I and Zn I abundances of $[\mathrm{Ni\,I/Fe}] = 0.09 \pm 0.13$ and $[\mathrm{Zn\,I/Fe}] = 0.01 \pm 0.15$ using 12 Ni lines and one Zn line. Comparison of these abundances to those of other UFD galaxy and MW halo stars (see Figure 2) reveals that the Cet II star has relatively low Ti and V abundances, while the remainder of the iron peak element abundances for this star are similar to those of other UFD galaxy and metal-poor MW halo stars.

4.4. Neutron-capture Elements

Absorption features from the two neutron-capture elements Sr and Ba were identified in the spectrum, and using spectral synthesis, we derive abundances for these elements of $[\mathrm{Sr\,II/Fe}] = -2.10 \pm 0.43$ and $[\mathrm{Ba\,II/Fe}] = -2.23 \pm 0.39$. The synthesis of the Sr 4077 and Ba 4554 Å lines are shown in Figure 4. The Sr abundance derived for J0117 is low and similar to what is found in most other UFD galaxies, and the Ba abundance is lower than the majority of other UFD galaxy stars (see Figure 3). No Eu could be detected in the spectrum, so we derive a 3σ upper limit of $[\mathrm{Eu\,II/Fe}] < -0.33$ from the 4129 Å line, which is plotted as a downward-pointing triangle in Figure 3.

5. Discussion

5.1. Nature of Cetus II

The nature of the Cet II overdensity is still debated in the literature. The DES discovery paper (Drlica-Wagner et al. 2015) and a more recent paper from the DES based on the analysis of more extensive photometry (Drlica-Wagner et al. 2020) both classify it as a probable UFD galaxy, while Conn et al. (2018), who presented GMOS-S photometry of the system, suggested that it is more likely a part of the Sagittarius (Sgr) tidal stream. However, the proper motion of the Cet II system, $(\mu_{\alpha\cos\delta}, \mu_\delta) = (+2.8 \pm 0.06, 0.5 \pm 0.06)$ mas yr^{-1} (Pace & Li 2019; Pace et al. 2022) does not agree with the proper motion of the Sgr stream $(\mu_{\alpha\cos\delta}, \mu_\delta) = (-1, -3)$ masyr^{-1} (Vasiliev et al. 2021) and therefore rules out an association with the Sgr stream. In addition to this, the velocity measured for J0117 does not agree with the velocity of the Sgr stream (Vasiliev et al. 2021), which further confirms that they are not associated. This will be explored in more detail in forthcoming work (J. D. Simon et al. 2023, in preparation).

The size of Cet II ($r_{1/2} \sim 17$pc; Drlica-Wagner et al. 2015) lies in an ambiguous region in the size–luminosity plane where the star cluster and UFD populations overlap (Willman & Strader 2012). As discussed in Willman & Strader (2012), the most effective classification for these systems is a velocity dispersion followed by a metallicity dispersion. These have not yet been measured for Cet II.

In this paper, we have derived the abundances of one star, J0117, in Cet II, and the general pattern of this star is similar to that of other UFD galaxy stars (see Figure 2) and is hence compatible with a UFD galaxy classification of Cet II. This is particularly supported by the very low abundance of the neutron-capture elements Sr and Ba, which have been found to be characteristic of UFD galaxies and can be used to classify a system (Ji et al. 2019), in particular, this abundance feature distinguishes UFD galaxy stars from GC stars. Furthermore, we suggest that a high K abundance is another potential UFD abundance signature, which is explored further in Section 5.2.2. No abundance analysis exists for Sgr stream stars at metallicities similar to J0117; however, there have been abundance analyses for stars in the Sgr dwarf spheroidal galaxy (dSph) at similar metallicities to J0117. The Sgr dSph stars show abundance signatures that we do not find in J0117, including higher neutron-capture element abundances ($-0.2 < [\mathrm{Sr/Fe}] < 0.6$, $-0.8 < [\mathrm{Ba/Fe}] < 0.8$, $-0.17 < [\mathrm{Eu/Fe}] < 0.81$ Hansen et al. 2018; Reichert et al. 2020). Thus, the chemical abundances of Cet II do not support an association with the Sgr dSph. For the remainder of the discussion, we adopt the classification of Cet II as a UFD galaxy.

5.2. Abundance Pattern of J0117

With its low metallicity, slight enhancement of the α-elements, and low abundances of neutron-capture elements, J0117 generally follows the same abundance trends seen in the majority of UFD galaxy stars. However, the derived

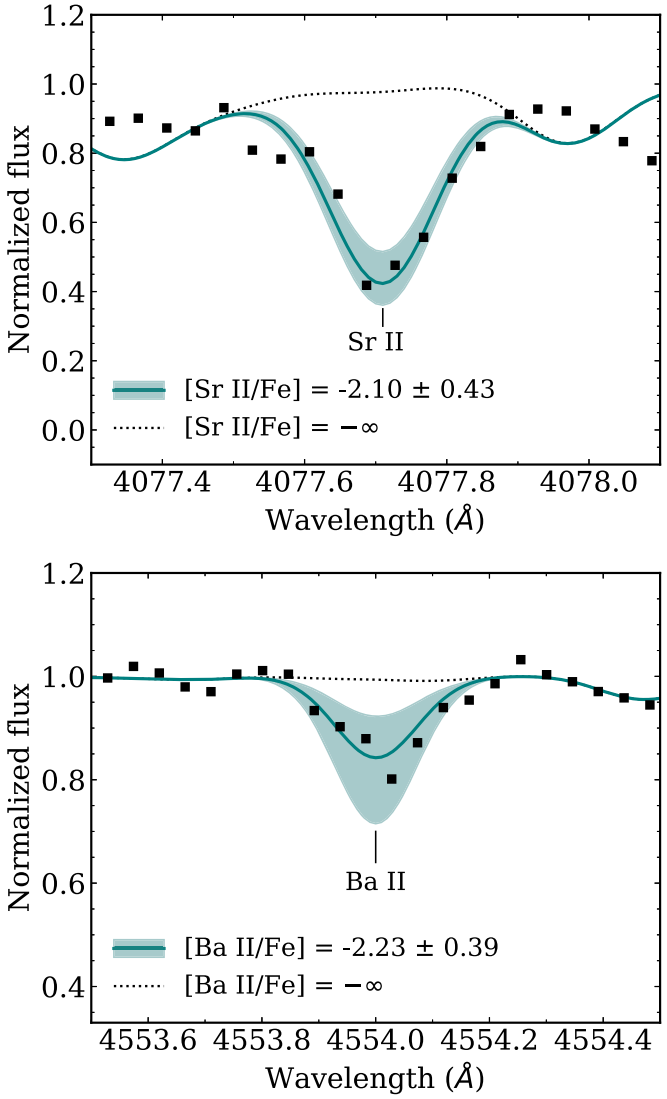

Figure 4. Spectral synthesis of the 4077 Å Sr II line (top) and 4554 Å Ba II line (bottom). The black squares show the observed spectrum of J0117. The dotted line shows a synthesis without Sr or Ba, and the blue line shows a synthesis with the [Sr/Fe] $\pm \sigma_{[Sr/Fe]}$ or [Ba/Fe] $\pm \sigma_{[Ba/Fe]}$ value derived for J0117.

abundances for some elements stand out and warrant further discussion.

5.2.1. Low Sc, Ti, and V Abundances

One specific feature of J0117 is that the [Sc/Fe], [Ti/Fe], and [V/Fe] ratios are ∼0.3, 0.2, and 0.1 dex lower, respectively, in this star than the average of what is seen in most other UFD galaxy stars and metal-poor MW halo stars (see Figure 2). We plot the 5657 Å Sc II and 5381 Å Ti II lines in the spectrum of J0117 (black) compared to spectra of stars HD 26297 (green) and BD+29 2356 (blue; I. Roederer, private communication) in Figure 5. HD 26297 and BD+29 2356 were chosen because they have similar model atmosphere parameters to J0117, but higher Sc and Ti abundances. However, it should be noted that there is a difference in [Fe/H] that amplifies the intrinsic difference in [Sc/Fe] and [Ti/Fe]. The parameters for each star and the abundances for each line are listed in Table 5. It is clear from Figure 5 that the absorption features of Sc and Ti are weaker in the spectrum of J0117, thus

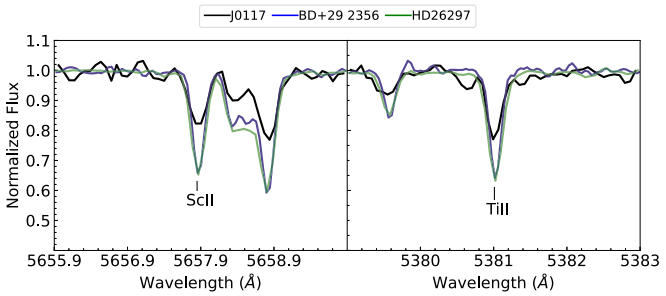

Figure 5. Comparison of the Sc II and Ti II absorption lines in J0117 to the MW halo stars BD+29 2356 and HD 26297 from Roederer et al. (2014). The absorption features for J0117 are weaker than what is seen for BD+29 2356 and HD 26297. The model atmosphere parameters and Sc and Ti abundances for each star are shown in Table 5.

supporting the lower abundances derived for these elements in this star.

The Sc, Ti, and V abundances for metal-poor stars have been investigated by Sneden et al. (2016), Cowan et al. (2020), and Ou et al. (2020), who all found that the abundances of these three elements are positively correlated in metal-poor stars ([Fe/H] < -2), indicating that these three elements have linked nucleosynthetic origins. While the main focus of Cowan et al. (2020) is the analysis of UV spectra taken with the Hubble Space Telescope of three metal-poor stars, they also investigated the correlation among the Sc, Ti, and V abundances derived in several large spectroscopic studies (e.g., Cayrel et al. 2004; Cohen et al. 2004, 2008; Barklem et al. 2005; Lai et al. 2008; Yong et al. 2013; Roederer et al. 2014), and found that the abundances reported in these studies also show correlations between the three elements.

Ti and V are produced via explosive Si- and O-burning in core-collapse SN (Woosley & Weaver 1995; Sneden et al. 2016), with models producing similar V/Ti ratios for both the Si and O SN ejecta components (e.g., Pignatari et al. 2016). Sneden et al. (2016) suggested that the correlation of the Ti and V abundances in metal-poor stars points to a coproduction of these elements, and that their abundances can be used to explore the properties of the progenitor and its explosion, such as the mass and explosion energy. The case of Sc is slightly more complicated. Although it can be produced in the same explosive Si- and O-burning layers (Woosley & Weaver 1995), it is more efficiently produced via neutrino feedback or during α-rich freeze-out conditions (Woosley & Weaver 1995; Fröhlich et al. 2006). This fact led Sneden et al. (2016) to argue that although a correlation is seen, the Sc/Ti and Sc/V ratios are less useful diagnostics than V/Ti ratios of the properties of the progenitor star. Generally, theoretical SN models often underproduce all three elements compared to the abundances derived from metal-poor stars (Kobayashi et al. 2020, and references therein). However, it was suggested by both Cowan et al. (2020) and Ou et al. (2020) that more energetic SN, such as hypernovae, might contribute to the abundances of these elements.

In contrast to the star analyzed in Sneden et al. (2016) and the three stars presented in Cowan et al. (2020), which all display higher than normal Sc, Ti, and V abundances, J0117 exhibits lower than average abundances for these elements. Because the chemistry of these stars is a direct fingerprint of the nucleosynthesis process of the first massive (Population III) stars to form in the galaxies, they can be used to constrain properties such as the mass range, rotation, and explosion

Table 5
Model Atmosphere Parameters and Sc and Ti Abundances for the Comparison Stars and J0117

ID	$T_{\rm eff}$ (K)	log g (cgs)	ξ (km s^{-1})	Model [Fe/H]	log ϵ(Sc II)	log ϵ(Ti II)
HD 26297	4400	1.10	1.75	−1.72	1.57	3.67
BD +29 2356	4710	1.75	1.50	−1.62	1.65	3.61
J0117	4727	1.40	1.89	−2.09	0.63	3.00

Note. Abundances for BD +29 2356 and HD 26297 are taken from Roederer et al. (2014).

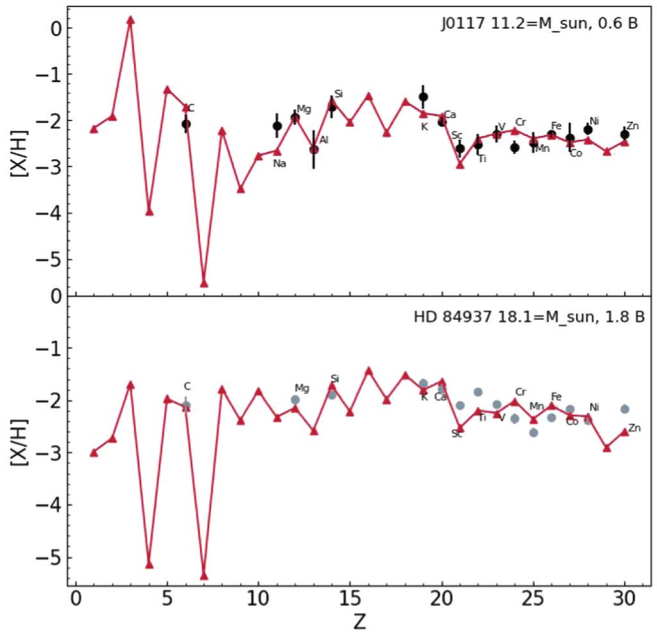

Figure 6. Best-fit SN yield model (Heger & Woosley 2010) for the derived abundances in J0117 (top) and HD 84937 (bottom). The black points are the derived abundances for J0117, the gray points are the derived abundances for HD 84937 (Sneden et al. 2016; Spite et al. 2017), and the red line is the best-fit SN yield model for each star.

energies of the Population III stars. To investigate the signature of J0117, we used the STARFIT tool[45] to match SN yields from Heger & Woosley (2010) to the abundances of J0117. The STARFIT code calculates a χ^2 statistic using the derived abundances and upper limits to determine the best-fit SN yields. For J0117, we obtained models with $\chi^2_{\rm red} < 2$, which returned models in a narrow range of progenitor masses, $M_\odot = 10.6$–13.6. The best fit ($\chi^2_{\rm red} = 1.12$) was achieved with a progenitor mass of $11.2 M_\odot$ and a modest explosion energy of 0.6 B.[46] Figure 6 shows the abundances for J0117 and best-fit model yields. This model provides a good fit to most elements, with only a few discrepancies. It should be noted that it is unlikely that this star was polluted by a singular Population III SN, but this tool gives an idea of the most dominant source of metals. To demonstrate the range of masses that can come from these abundances, we also derived the best-fit yields for the star from Sneden et al. (2016), HD 84937. HD 84937 is used for comparison because it has high Sc, Ti, and V abundances compared to the average halo stars and thus represents the high end of the abundance distribution, with J0117 representing the low end. The abundances for the light elements were taken from Spite et al. (2017), who adopted similar stellar parameters for HD 84937 as Sneden et al. (2016). For HD 84937, the best fit was achieved with a progenitor mass of $18.1 M_\odot$ and an explosion energy of 1.8 B. This demonstrates that the abundances for these elements can be used to gain information about the progenitor masses and explosion energies as well as how these parameters can vary with different abundances. Furthermore, the progenitor mass found for the Cet II star is also somewhat lower than what has been found for stars in other UFD galaxies (Hansen et al. 2020), pointing to a wide range of progenitor masses in UFD galaxies.

Another possibility to explain the low Sc and V abundances that we see is pollution from Type Ia SN. As seen in Bravo et al. (2019), the production of Sc and V in Type Ia SN is metallicity dependent and decreases with decreasing metallicity. Hence, it is possible that the low Sc and V abundances are a result of increased Fe injection from Type Ia SN with low Sc and V production. However, the α-element abundance ratios in J0117 are slightly enhanced and compatible with core-collapse SN production, and they do not suggest additional Fe injection from Type Ia SN.

5.2.2. High K Abundance

Another peculiar feature of J0117 is the somewhat high [K/Fe] abundance of 0.81 derived for this star. As can be seen in Figure 2, however, J0117 is not a complete outlier. High K has been found in several other UFD galaxy stars. In fact, in Figure 2, it can be seen that stars in UFD galaxies generally have higher [K/Fe] ratios than MW halo stars at similar metallicity. However, K is known to suffer from nonlocal thermodynamic equilibrium (NLTE) effects (de La Reza & Mueller 1975). We therefore corrected the K abundance derived for J0117 and the K abundances of the UFD galaxy literature sample following the study of Reggiani et al. (2019) and obtained a [K/Fe] abundance of 0.64 for J0117. The NLTE-corrected K abundances for J0117 and other UFD galaxy stars, along with NLTE-corrected K abundances of halo stars (Roederer et al. 2014), are shown in the middle panel of Figure 7, while the LTE abundances are shown in the panel on the left. It can be seen that the offset between a subset of the UFD galaxies and the halo stars remains after the correction is applied. Ivanova & Shimanskiĭ (2000) also looked at the NLTE corrections for K and provided corrections slightly larger than Reggiani et al. (2019). However, even with these corrections, the offset between the MW halo stars and a subset of the UFD galaxies remains.

Apart from the NLTE effects, the K lines also have hyperfine structure. However, this is very weak and therefore generally not included in the abundance analysis. For completeness, however, we derived K abundances from the two lines used above via spectral synthesis, including the hyperfine structure. As expected, the effect on the abundances was minimum

[45] https://starfit.org/
[46] B = 1 Bethe = 10^{51} erg.

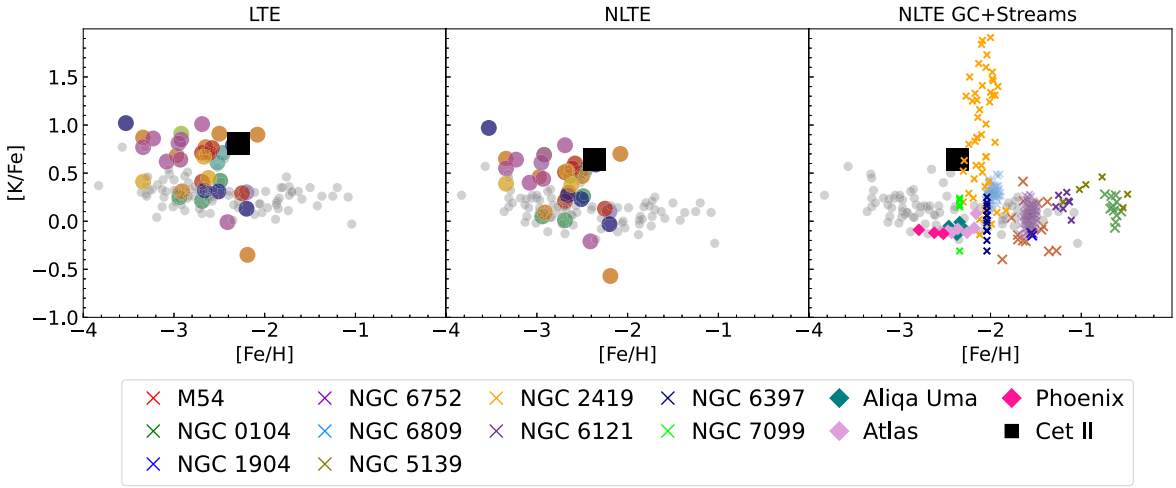

Figure 7. Left: LTE [K/Fe] abundances for J0117 (black square), UFDs (colored dots; see Figure 2 for the legend), and MW halo (gray dots) stars. Middle: NLTE-corrected [K/Fe] abundances for J0117, UFDs, and MW halo stars. Right: NLTE-corrected [K/Fe] abundances for J0117, MW halo stars, GC stars (colored x), and stars from stellar streams with GC progenitor (colored diamonds). There is an offset in [K/Fe] abundance between some UFD galaxies and the average value for MW halo stars. The GC and stellar stream [K/Fe] abundances also mostly overlap with the MW halo stars and are lower than what is seen in UFD galaxy stars.

(<0.1). Hence, for compatibility with the literature data, the discussion below is based on our K abundance derived from the EW analysis.

Although the abundances of J0117 are compatible with Cet II being a UFD galaxy, we searched the literature for K abundances in GCs to explore whether this abundance signature is unique to stars in UFD galaxies or if can be found in other types of small stellar systems. The results of this exercise are plotted in the right panel of Figure 7, where the GC NLTE-corrected K abundances for stars in ten GCs (M54 (Carretta 2022), NGC 2419 (Mucciarelli et al. 2012), NGC 104, NGC 6809 (Mucciarelli et al. 2017), NGC 6752 (Carretta et al. 2007), NGC 1904, NGC 5139, NGC 6121, NGC 6397, and NGC 7099 (Carretta et al. 2013) are marked with crosses. As can be seen, for most GCs, the K abundances overlap with the halo stars, suggesting that the high K abundances seen in UFD galaxy stars may be a unique abundance signature of these systems. The exception is NGC 2419, in which stars with a wide range of K abundances are found, including K-rich ([K/Fe] > 1) stars. However, the K-rich stars in this cluster are all Mg-poor ([Mg/Fe] < 0; Cohen & Kirby 2012; Mucciarelli et al. 2012), thus making them distinguishable from the UFD galaxy stars, which usually exhibit a small enhancement in Mg (J0117, e.g., has [Mg/Fe] = 0.36). Although we find K abundances in a number of GCs, most have metallicities higher than the UFD galaxy stars with K abundances, hampering a direct comparison. However, in recent years, a number of stellar streams have been detected that are thought to be the remnants of more metal-poor GCs accreted by the MW, such as the Phoenix, Aliqa Uma, and ATLAS streams (Li et al. 2019, 2022; Wan et al. 2020; Casey et al. 2021). Ji et al. (2020) derived K abundances for stars in the three GC streams listed above. These abundances are plotted as diamonds in Figure 7. Similar to the present-day GCs, the stream stars also have K abundances overlapping with the MW halo stars. Hence, high K abundances seem to be a characteristic abundance signature for at least some UFD galaxies.

The nucleosynthetic origin of the high K abundances seen in UFD galaxy stars is so far unknown. K is created through hydrostatic oxygen-shell burning and explosive oxygen burning with yields depending on the progenitor mass (Woosley & Weaver 1995). Recently, models have shown that K production is increased when rotation is introduced (Prantzos et al. 2018). Hence, the high K abundances in UFD galaxy stars could suggest that some of these stars were enriched by massive rotating stars. The models also show low Sc production in massive rotating stars (Prantzos et al. 2018), which is in agreement with the Sc in J0117 ([Sc/Fe] = −0.31). However, it is not a good fit for the other UFD stars that do not have low Sc.

Since the high K abundances are mainly seen in the UFD galaxy stars, it is possible that this signature is tied to the slow chemical evolution of these systems. Although unlikely given the overall abundance signature of J0117, the K could also come from a nucleosynthesis source with a time-delayed contribution, like Type Ia SN. One candidate could be Ca-rich transients (Kasliwal et al. 2012), the light curves of which Polin et al. (2021) recently found to match models of sub-Chandrasekhar Type Ia SNe with low-mass progenitors. However, more modeling is needed to establish whether these events can contribute to the K abundances of UFD galaxy stars.

6. Summary

We have performed a detailed chemical abundance analysis of J0117, the brightest star of the Cet II UFD galaxy candidate. Our analysis shows that this star is a metal-poor, α-enhanced (α-elements $\gtrsim$0.4) star with low abundances of the neutron-capture elements ([Sr/Fe] = −2.10 and [Ba/Fe] = −2.23), following the trends seen for the chemical analysis of other UFD galaxy stars. Thus, although the classification of this system is still debated, the results of this chemical analysis suggest that Cet II is a UFD galaxy. Further observations and chemical analysis of more stars in this system will help us to fully determine the nature of Cet II. The analysis revealed that the star exhibits slightly lower [Sc/Fe], [Ti/Fe], and [V/Fe] abundances than other UFD galaxy and MW halo stars at similar metallicities. It has been suggested that the abundances for [Sc/Fe], [Ti/Fe], and [V/Fe] can be used as a diagnostic for progenitor mass; we thus compared the abundances of J0117 with the Heger & Woosley (2010) SNe yields and determined a best fit with a progenitor mass of 11.2$M_{\odot}$, somewhat lower than the progenitor masses found for stars in other UFD galaxies (Hansen et al. 2020). Finally, we derive a

K abundance of [K/Fe] = 0.81 for J0117, which, even after it has been corrected for NLTE effects, is somewhat higher than the K abundances derived for MW halo stars at similar metallicities. We note that a number of UFD galaxies have high K abundances compared to the MW halo stars, and by including K abundances for stars in GCs and streams in our comparison, we find that this is a unique signature of some UFD galaxy stars.

Acknowledgments

The authors would like to thank Dr. Maria Drout for collecting the spectra of J0117 from 2017 November and Dr. Andrew McWilliam for atomic K line data and insightful comments on K abundances in stars.

This research made extensive use of the SIMBAD database operated at CDS, Straasburg, France (Wenger et al. 2000), https://arxiv.org/, and NASA's Astrophysics Data System for bibliographic information.

Funding for the DES Projects has been provided by the U.S. Department of Energy, the U.S. National Science Foundation, the Ministry of Science and Education of Spain, the Science and Technology Facilities Council of the United Kingdom, the Higher Education Funding Council for England, the National Center for Supercomputing Applications at the University of Illinois at Urbana-Champaign, the Kavli Institute of Cosmological Physics at the University of Chicago, the Center for Cosmology and Astro-Particle Physics at the Ohio State University, the Mitchell Institute for Fundamental Physics and Astronomy at Texas A&M University, Financiadora de Estudos e Projetos, Fundação Carlos Chagas Filho de Amparo à Pesquisa do Estado do Rio de Janeiro, Conselho Nacional de Desenvolvimento Científico e Tecnológico and the Ministério da Ciência, Tecnologia e Inovação, the Deutsche Forschungsgemeinschaft and the Collaborating Institutions in the Dark Energy Survey.

The Collaborating Institutions are Argonne National Laboratory, the University of California at Santa Cruz, the University of Cambridge, Centro de Investigaciones Energéticas, Medioambientales y Tecnológicas-Madrid, the University of Chicago, University College London, the DES-Brazil Consortium, the University of Edinburgh, the Eidgenössische Technische Hochschule (ETH) Zürich, Fermi National Accelerator Laboratory, the University of Illinois at Urbana-Champaign, the Institut de Ciències de l'Espai (IEEC/CSIC), the Institut de Física d'Altes Energies, Lawrence Berkeley National Laboratory, the Ludwig-Maximilians Universität München and the associated Excellence Cluster Universe, the University of Michigan, NSF's NOIRLab, the University of Nottingham, The Ohio State University, the University of Pennsylvania, the University of Portsmouth, SLAC National Accelerator Laboratory, Stanford University, the University of Sussex, Texas A&M University, and the OzDES Membership Consortium.

Based in part on observations at Cerro Tololo Inter-American Observatory at NSF's NOIRLab (NOIRLab Prop. ID 2012B-0001; PI: J. Frieman), which is managed by the Association of Universities for Research in Astronomy (AURA) under a cooperative agreement with the National Science Foundation.

The DES data management system is supported by the National Science Foundation under grant Nos. AST-1138766 and AST-1536171. The DES participants from Spanish institutions are partially supported by MICINN under grants ESP2017-89838, PGC2018-094773, PGC2018-102021, SEV-2016-0588, SEV-2016-0597, and MDM-2015-0509, some of which include ERDF funds from the European Union. IFAE is partially funded by the CERCA program of the Generalitat de Catalunya. Research leading to these results has received funding from the European Research Council under the European Union's Seventh Framework Program (FP7/2007-2013) including ERC grant agreements 240672, 291329, and 306478. We acknowledge support from the Brazilian Instituto Nacional de Ciência e Tecnologia (INCT) do e-Universo (CNPq grant 465376/2014-2).

This manuscript has been authored by Fermi Research Alliance, LLC under Contract No. DE-AC02-07CH11359 with the U.S. Department of Energy, Office of Science, Office of High Energy Physics. T.T.H acknowledges support from the Swedish Research Council (VR 2021-05556).

Facility: Magellan:Clay.

Software: MOOG (Sneden 1973; Sobeck et al. 2011), IRAF (Tody 1986, 1993), ATLAS9 (Castelli & Kurucz 2003), linemake (Placco et al. 2021), NumPy (van der Walt et al. 2011), Matplotlib (Hunter 2007), AstroPy (Astropy Collaboration et al. 2013, 2018), CarPy (Kelson 2003), SMHR (Casey 2014).

ORCID iDs

K. B. Webber https://orcid.org/0000-0002-9762-4308
T. T. Hansen https://orcid.org/0000-0001-6154-8983
J. D. Simon https://orcid.org/0000-0002-4733-4994
A. B. Pace https://orcid.org/0000-0002-6021-8760
B. Mutlu-Pakdil https://orcid.org/0000-0001-9649-4815
A. Drlica-Wagner https://orcid.org/0000-0001-8251-933X
C. E. Martínez-Vázquez https://orcid.org/0000-0002-9144-7726
M. Aguena https://orcid.org/0000-0001-5679-6747
S. S. Allam https://orcid.org/0000-0002-7069-7857
O. Alves https://orcid.org/0000-0002-7394-9466
E. Bertin https://orcid.org/0000-0002-3602-3664
D. Brooks https://orcid.org/0000-0002-8458-5047
A. Carnero Rosell https://orcid.org/0000-0003-3044-5150
J. Carretero https://orcid.org/0000-0002-3130-0204
L. N. da Costa https://orcid.org/0000-0002-7731-277X
J. De Vicente https://orcid.org/0000-0001-8318-6813
I. Ferrero https://orcid.org/0000-0002-1295-1132
D. Friedel https://orcid.org/0000-0002-3632-7668
J. Frieman https://orcid.org/0000-0003-4079-3263
J. García-Bellido https://orcid.org/0000-0002-9370-8360
G. Giannini https://orcid.org/0000-0002-3730-1750
D. Gruen https://orcid.org/0000-0003-3270-7644
R. A. Gruendl https://orcid.org/0000-0002-4588-6517
S. R. Hinton https://orcid.org/0000-0003-2071-9349
D. L. Hollowood https://orcid.org/0000-0002-9369-4157
K. Honscheid https://orcid.org/0000-0002-6550-2023
K. Kuehn https://orcid.org/0000-0003-0120-0808
J. Mena-Fernández https://orcid.org/0000-0001-9497-7266
F. Menanteau https://orcid.org/0000-0002-1372-2534
R. Miquel https://orcid.org/0000-0002-6610-4836
R. L. C. Ogando https://orcid.org/0000-0003-2120-1154
M. E. S. Pereira https://orcid.org/0000-0002-7131-7684
A. Pieres https://orcid.org/0000-0001-9186-6042
A. A. Plazas Malagón https://orcid.org/0000-0002-2598-0514
E. Sanchez https://orcid.org/0000-0002-9646-8198
J. Allyn Smith https://orcid.org/0000-0002-6261-4601
M. Smith https://orcid.org/0000-0002-3321-1432
E. Suchyta https://orcid.org/0000-0002-7047-9358

G. Tarle https://orcid.org/0000-0003-1704-0781
C. To https://orcid.org/0000-0001-7836-2261
N. Weaverdyck https://orcid.org/0000-0001-9382-5199
B. Yanny https://orcid.org/0000-0002-9541-2678

References

Asplund, M., Grevesse, N., Sauval, A. J., et al. 2009, ARA&A, 47, 481
Astropy Collaboration, Price-Whelan, A. M., Sipőcz, B. M., et al. 2018, AJ, 156, 123
Astropy Collaboration, Robitaille, T. P., Tollerud, E. J., et al. 2013, A&A, 558, A33
Barklem, P. S., Christlieb, N., Beers, T. C., et al. 2005, A&A, 439, 129
Bechtol, K., Drlica-Wagner, A., Balbinot, E., et al. 2015, ApJ, 807, 50
Belmonte, M. T., Pickering, J. C., Ruffoni, M. P., et al. 2017, ApJ, 848, 125
Bernstein, R., Shectman, S. A., Gunnels, S. M., et al. 2003, Proc. SPIE, 4841, 1694
Bravo, E., Badenes, C., & Martínez-Rodríguez, H. 2019, MNRAS, 482, 4346
Cantu, S. A., Pace, A. B., Marshall, J., et al. 2021, ApJ, 916, 81
Carretta, E. 2022, A&A, 666, A177
Carretta, E., Bragaglia, A., Gratton, R. G., et al. 2007, yCat, J/A+A/464/927
Carretta, E., Bragaglia, A., Gratton, R. G., et al. 2010, A&A, 516, A55
Carretta, E., Gratton, R. G., Bragaglia, A., et al. 2013, ApJ, 769, 40
Casagrande, L., Ramírez, I., Meléndez, J., et al. 2010, A&A, 512, A54
Casey, A. R. 2014, *PhD Thesis*., Australian National Univ.
Casey, A. R., Ji, A. P., Hansen, T. T., et al. 2021, ApJ, 921, 67
Castelli, F., & Kurucz, R. L. 2003, in IAU Symp. 210, Modeling of Stellar Atmospheres, ed. N. Piskunov, W. W. Weiss, & D. F. Gray (Cambridge: Cambridge Univ. Press), A20
Cayrel, R., Depagne, E., Spite, M., et al. 2004, A&A, 416, 1117
Chiti, A., Frebel, A., Ji, A. P., et al. 2018, ApJ, 857, 74
Chiti, A., Frebel, A., Ji, A. P., et al. 2023, AJ, 165, 55
Cohen, J. G., Christlieb, N., McWilliam, A., et al. 2004, ApJ, 612, 1107
Cohen, J. G., Christlieb, N., McWilliam, A., et al. 2008, ApJ, 672, 320
Cohen, J. G., & Kirby, E. N. 2012, ApJ, 760, 86
Conn, B. C., Jerjen, H., Kim, D., et al. 2018, ApJ, 857, 70
Cowan, J. J., Sneden, C., Roederer, I. U., et al. 2020, ApJ, 890, 119
de La Reza, R., & Mueller, E. A. 1975, SoPh, 43, 15
Den Hartog, E. A., Lawler, J. E., Sneden, C., et al. 2019, ApJS, 243, 33
Den Hartog, E. A., Lawler, J. E., Sobeck, J. S., et al. 2011, ApJS, 194, 35
Den Hartog, E. A., Ruffoni, M. P., Lawler, J. E., et al. 2014, ApJS, 215, 23
Dotter, A., Chaboyer, B., Jevremović, D., et al. 2008, ApJS, 178, 89
Dressler, A., Bigelow, B., Hare, T., et al. 2011, PASP, 123, 288
Drlica-Wagner, A., Bechtol, K., Mau, S., et al. 2020, ApJ, 893, 47
Drlica-Wagner, A., Bechtol, K., Rykoff, E. S., et al. 2015, ApJ, 813, 109
Drlica-Wagner, A., Sevilla-Noarbe, I., Rykoff, E. S., et al. 2018, ApJS, 235, 33
Feltzing, S., Eriksson, K., Kleyna, J., et al. 2009, A&A, 508, L1
Frebel, A., Casey, A. R., Jacobson, H. R., et al. 2013, ApJ, 769, 57
Frebel, A., & Norris, J. E. 2015, ARA&A, 53, 631
Frebel, A., Norris, J. E., Gilmore, G., et al. 2016, ApJ, 826, 110
Frebel, A., Simon, J. D., Geha, M., et al. 2010, ApJ, 708, 560
Frebel, A., Simon, J. D., & Kirby, E. N. 2014, ApJ, 786, 74
Fröhlich, C., Hauser, P., Liebendörfer, M., et al. 2006, ApJ, 637, 415
Gaia Collaboration, Brown, A. G. A., Vallenari, A., et al. 2021, A&A, 649, A1
Gilmore, G., Norris, J. E., Monaco, L., et al. 2013, ApJ, 763, 61
Hansen, C. J., El-Souri, M., Monaco, L., et al. 2018, ApJ, 855, 83
Hansen, T. T., Marshall, J. L., Simon, J. D., et al. 2020, ApJ, 897, 183
Hansen, T. T., Simon, J. D., Marshall, J. L., et al. 2017, ApJ, 838, 44
Hayes, C. R., Venn, K. A., Waller, F., et al. 2023, ApJ, 955, 17
Heger, A., & Woosley, S. E. 2010, ApJ, 724, 341
Hunter, J. D. 2007, CSE, 9, 90
Ishigaki, M. N., Aoki, W., Arimoto, N., et al. 2014, A&A, 562, A146
Ivanova, D. V., & Shimanskiĭ, V. V. 2000, ARep, 44, 376
Ji, A. P., Frebel, A., Chiti, A., et al. 2016, Natur, 531, 610
Ji, A. P., Frebel, A., Ezzeddine, R., et al. 2016, ApJL, 832, L3
Ji, A. P., Frebel, A., Simon, J. D., et al. 2016, ApJ, 830, 93
Ji, A. P., Frebel, A., Simon, J. D., et al. 2016, ApJ, 817, 41
Ji, A. P., Li, T. S., Hansen, T. T., et al. 2020, AJ, 160, 181
Ji, A. P., Li, T. S., Simon, J. D., et al. 2020, ApJ, 889, 27
Ji, A. P., Simon, J. D., Frebel, A., et al. 2019, ApJ, 870, 83
Ji, A. P., Simon, J. D., Roederer, I. U., et al. 2022, ApJ, 165, 100
Kasliwal, M. M., Kulkarni, S. R., Gal-Yam, A., et al. 2012, ApJ, 755, 161
Kelson, D. D. 2003, PASP, 115, 688
Kelson, D. D., Illingworth, G. D., van Dokkum, P. G., et al. 2000, ApJ, 531, 159
Kobayashi, C., Karakas, A. I., & Lugaro, M. 2020, ApJ, 900, 179
Koch, A., McWilliam, A., Grebel, E. K., et al. 2008, ApJL, 688, L13
Koposov, S. E., Belokurov, V., Torrealba, G., et al. 2015, ApJ, 805, 130
Kramida, A., Ralchenko, Y., Nave, G., et al. 2018, APS Division of Atomic and Molecular Physics Meeting 2018, M01.004, http://meetings.aps.org/link/BAPS.2018.DAMOP.M01.4
Krumholz, M. R., McKee, C. F., & Bland-Hawthorn, J. 2019, ARA&A, 57, 227
Kurucz, R. L., & Bell, B. 1995, Kurucz CD-ROM (Cambridge, MA: Smithsonian Astrophysical Obs.)
Laevens, B. P. M., Martin, N. F., Bernard, E. J., et al. 2015, ApJ, 813, 44
Laevens, B. P. M., Martin, N. F., Sesar, B., et al. 2014, ApJL, 786, L3
Lai, D. K., Bolte, M., Johnson, J. A., et al. 2008, ApJ, 681, 1524
Lai, D. K., Lee, Y. S., Bolte, M., et al. 2011, ApJ, 738, 51
Lawler, J. E., & Dakin, J. T. 1989, JOSAB, 6, 1457
Lawler, J. E., Guzman, A., Wood, M. P., et al. 2013, ApJS, 205, 11
Lawler, J. E., Sneden, C., & Cowan, J. J. 2015, ApJS, 220, 13
Lawler, J. E., Sneden, C., Nave, G., et al. 2017, ApJS, 228, 10
Lawler, J. E., Wood, M. P., Den Hartog, E. A., et al. 2014, ApJS, 215, 20
Li, T. S., Ji, A. P., Pace, A. B., et al. 2022, ApJ, 928, 30
Li, T. S., Koposov, S. E., Zucker, D. B., et al. 2019, MNRAS, 490, 3508
Luque, E., Santiago, B., Pieres, A., et al. 2018, MNRAS, 478, 2006
Marshall, J. L., Hansen, T., Simon, J. D., et al. 2019, ApJ, 882, 177
McWilliam, A. 1998, AJ, 115, 1640
Meléndez, J., & Barbuy, B. 2009, A&A, 497, 611
Mucciarelli, A., Bellazzini, M., Ibata, R., et al. 2012, MNRAS, 426, 2889
Mucciarelli, A., Lapenna, E., Ferraro, F. R., et al. 2018, ApJ, 859, 75
Mucciarelli, A., Merle, T., & Bellazzini, M. 2017, yCat, J/A+A/600/A104
Norris, J. E., Wyse, R. F. G., Gilmore, G., et al. 2010, ApJ, 723, 1632
O'Brian, T. R., Wickliffe, M. E., Lawler, J. E., et al. 1991, JOSAB, 8, 1185
Ou, X., Roederer, I. U., Sneden, C., et al. 2020, ApJ, 900, 106
Pace, A. B., Erkal, D., & Li, T. S. 2022, ApJ, 940, 136
Pace, A. B., & Li, T. S. 2019, ApJ, 875, 77
Pehlivan Rhodin, A., Hartman, H., Nilsson, H., et al. 2017, A&A, 598, A102
Pickering, J. C., Thorne, A. P., & Perez, R. 2001, ApJS, 132, 403
Pickering, J. C., Thorne, A. P., & Perez, R. 2002, ApJS, 138, 247
Pignatari, M., Herwig, F., Hirschi, R., et al. 2016, ApJS, 225, 24
Placco, V. M., Frebel, A., Beers, T. C., et al. 2014, ApJ, 797, 21
Placco, V. M., Sneden, C., Roederer, I. U., et al. 2021, RNAAS, 5, 92
Polin, A., Nugent, P., & Kasen, D. 2021, ApJ, 906, 65
Prantzos, N., Abia, C., Limongi, M., et al. 2018, MNRAS, 476, 3432
Reggiani, H., Amarsi, A. M., Lind, K., et al. 2019, A&A, 627, A177
Reichert, M., Hansen, C. J., Hanke, M., et al. 2020, A&A, 641, A127
Roederer, I. U., & Kirby, E. N. 2014, MNRAS, 440, 2665
Roederer, I. U., & Lawler, J. E. 2012, ApJ, 750, 76
Roederer, I. U., Mateo, M., Bailey, J. I., et al. 2016, AJ, 151, 82
Roederer, I. U., Preston, G. W., Thompson, I. B., et al. 2014, AJ, 147, 136
Ruffoni, M. P., Den Hartog, E. A., Lawler, J. E., et al. 2014, MNRAS, 441, 3127
Simon, J. D. 2019, ARA&A, 57, 375
Simon, J. D., Frebel, A., McWilliam, A., et al. 2010, ApJ, 716, 446
Simon, J. D., & Geha, M. 2007, ApJ, 670, 313
Sneden, C., Cowan, J. J., & Gallino, R. 2008, ARA&A, 46, 241
Sneden, C., Cowan, J. J., Kobayashi, C., et al. 2016, ApJ, 817, 53
Sneden, C. A. 1973, *PhD Thesis*, Univ. Texas at Austin
Sobeck, J. S., Kraft, R. P., Sneden, C., et al. 2011, AJ, 141, 175
Sobeck, J. S., Lawler, J. E., & Sneden, C. 2007, ApJ, 667, 1267
Spite, M., Peterson, R. C., Gallagher, A. J., et al. 2017, A&A, 600, A26
Spite, M., Spite, F., François, P., et al. 2018, A&A, 617, A56
The Dark Energy Survey Collaboration 2005, arXiv:astro-ph/0510346
Tody, D. 1986, Proc. SPIE, 627, 733
Tody, D. 1993, in ASP Conf. Ser. 52, Astronomical Data Analysis Software and Systems II, ed. R. J. Hanisch (San Francisco, CA: ASP), 173
Trumpler, R. J. 1930, LicOB, 420, 154
van der Walt, S., Colbert, S. C., & Varoquaux, G. 2011, CSE, 13, 22
Vasiliev, E., Belokurov, V., & Erkal, D. 2021, MNRAS, 501, 2279
Waller, F., Venn, K., Sestito, F., et al. 2022, MNRAS, 519, 1349
Wan, Z., Lewis, G. F., Li, T. S., et al. 2020, Natur, 583, 768
Wenger, M., Ochsenbein, F., Egret, D., et al. 2000, A&AS, 143, 9
Willman, B., & Strader, J. 2012, AJ, 144, 76
Wood, M. P., Lawler, J. E., Den Hartog, E. A., et al. 2014, ApJS, 214, 18
Wood, M. P., Lawler, J. E., Sneden, C., et al. 2013, ApJS, 208, 27
Wood, M. P., Lawler, J. E., Sneden, C., et al. 2014, ApJS, 211, 20
Woosley, S. E., & Weaver, T. A. 1995, ApJS, 101, 181
Yong, D., Norris, J. E., Bessell, M. S., et al. 2013, ApJ, 762, 26
Yu, Y., & Derevianko, A. 2018, ADNDT, 119, 263